Title

Stent and Leaflet Stresses in 29-mm Second-Generation Balloon-Expandable Transcatheter Aortic Valve

Journal

The Annals of Thoracic Surgery, 104(3)

ISSN

0003-4975

Authors

Xuan, Yue
Krishnan, Kapil
Ye, Jian
et al.

Publication Date

2017-09-01

DOI

10.1016/j.athoracsur.2017.01.064

Peer reviewed

HHS Public Access

Author manuscript

Ann Thorac Surg. Author manuscript; available in PMC 2018 March 06.

Published in final edited form as:

Ann Thorac Surg. 2017 September ; 104(3): 773–781. doi:10.1016/j.athoracsur.2017.01.064.

Stent and Leaflet Stresses in 29mm Second Generation Balloon-Expandable Transcatheter Aortic Valve

Yue Xuan, PhD[1], **Kapil Krishnan, PhD**[1], **Jian Ye, MD**[2], **Danny Dvir, MD**[3], **Hesam Moghaddam, PhD**[1], **Julius M. Guccione, PhD**[1], **Liang Ge, PhD**[1], and **Elaine E. Tseng, MD**[1]

[1]Department of Surgery, University of California San Francisco and San Francisco VA Medical Centers, San Francisco, CA

[2]Division of Cardiovascular Surgery, St. Paul's Hospital and Vancouver General Hospital, Vancouver, BC, Canada

[3]Division of Cardiology, University of Washington, Seattle, WA

Abstract

Background—Equipoise of transcatheter aortic valve replacement (TAVR) with surgical aortic valve replacement (SAVR) in intermediate-risk patients has been demonstrated. As TAVR usage expands, questions regarding long-term durability become paramount. Valve design impacts durability with regions of increased leaflet stress being vulnerable to early failure. However, transcatheter aortic valve (TAV) leaflet stresses are unknown. The objective of this study was to determine stent and leaflet stresses of second generation balloon-expandable TAV.

Methods—Commercial 29mm Edwards Sapien XT underwent high-resolution micro-computed tomography scanning to develop precise 3D geometric mesh. Compressed and uncompressed TAVs were modeled under systemic pressure using finite element software. Material properties of stent were based on cobalt-chromium, while those for leaflets were obtained from surgical bioprostheses.

Results—Maximum and minimum principal stresses on uncompressed Sapien XT TAV were 1.63MPa and −0.36MPa on leaflets and 93.3Mpa and −105.6MPa on stent at diastolic pressure. Peak leaflet stress was observed at commissural tips where leaflets connected to the stent. For compressed TAV to 26mm, maximum and minimum principal stresses were 1.55MPa and −0.63MPa on leaflets and 526.1MPa and −902.2MPa on stent at diastolic pressure. Peak leaflet stress was located at similar position and also along the suture line with the dacron.

Conclusions—Stress analysis of two extreme deployed geometries of 29mm Edwards Sapien XT using exact geometry from high-resolution scans demonstrated that peak stresses for TAV leaflets were present at commissural tips where leaflets were attached. These regions would be mostly likely to initiate degeneration.

Corresponding Author: Elaine E. Tseng, MD, Professor, Division of Cardiothoracic Surgery, University of California San Francisco and San Francisco VA Medical Center, 4150 Clement St. 112D, San Francisco, CA 94121, Office: 415-221-4810 x23452, Fax: 415-750-2181, Elaine.Tseng@ucsf.edu.

Presented as poster at the Transcatheter Cardiovascular Therapeutics, October, 2015, San Francisco, CA, USA.

Classifications

Transcatheter aortic valve; biomechanics; bioprosthetic degeneration

Introduction

Transcatheter aortic valve replacement (TAVR) has proven effective therapy for severe aortic stenosis (AS) in high-risk surgical and inoperable patients[1]. At 5 years, Placement of Aortic Transcatheter Valves (PARTNER) randomized trials demonstrated sustained survival improvement of TAVR over medical therapy for inoperable patients and clinical equipoise for mortality between TAVR and surgical aortic valve replacement (SAVR) in high-risk patients[2,3]. Similarly, CoreValve US Extreme Risk randomized study showed similar survival benefit of self-expanding TAVR at 1 year[4]. For high-risk surgical patients, CoreValve US High Risk randomized study demonstrated TAVR superiority over SAVR in mortality at 1 year with ~5% absolute risk reduction[5]. PARTNER II has recently demonstrated equipoise of TAVR and SAVR in intermediate-risk patients which has further expanded TAVR indications[6]. Meanwhile, paravalvular leakage has been significantly reduced with introduction of Federal Drug Administration approved Sapien3 (Edwards Lifesciences, Inc, Irvine, CA). However, as TAVR practice continues to expand to eventually low-risk patients as reported in the Nordic Aortic Valve Intervention Trial (NOTION)[7], one enduring concern remains—TAVR long-term durability, which cannot be answered by current clinical trials. Concerns of TAVR durability have not been an issue in the original high-risk and inoperable cohorts whose enrolled patients were typically octagenarians[2–5] However, as lower-risk younger patients become enrolled, TAVR durability must be considered.

Clinically, relative TAVR durability among different devices or compared to surgical bioprosthesis is unknown. With respect to valve leaflet composition, surgical bioprostheses use bovine pericardium, porcine valve leaflets, or human allograft valves. TAVR has been designed using bovine, porcine, or equine pericardium, or porcine leaflets[8]. However, due to size constraints within 14–18Fr TAVR delivery systems[8], TAVR leaflets are much thinner than those of surgical bioprostheses[9,10]. Understanding TAVR leaflet stresses is important for determining durability; however, TAVR leaflet stresses are unknown and impossible to directly measure. The goal of this study was to determine TAV stent and leaflet stresses in 29mm second generation Edwards SapienXT (Edwards Lifesciences, Inc, Irvine, CA) using finite element analyses (FEA). FEA is a commonly used approach to predict durability and stability of complicated real-world systems such as bridges and buildings. FEA in physiologic studies is particularly useful when applied to device design to determine stresses that would otherwise be impossible to directly measure, and failure modes. Finite element (FE) models require accurate three-dimensional geometry in zero-stress state, material properties, and physiologic loading conditions. Previous FEA studies of TAVR used generic estimated leaflet geometry based on surgical valves, or homemade TAVs[10–12]. Furthermore, patient-specific FEA simulations have focused on interaction of TAVR stent with surrounding aortic root geometry but not on precise TAVR leaflet

geometry[12–18]. Our study focuses on TAVR stresses using high resolution imaging of SapienXT to obtain accurate 3D geometry for FEA.

Materials and Methods

Commercial 29mm Edwards SapienXT (external diameter 29mm, height 19.1mm) was obtained. TAV consisted of 3 components: cobalt-chromium stent, dacron covering, and bovine pericardial leaflets. Determining TAV stress distribution required: 1) development of TAV mesh using 3D geometry, 2) FEA using FE explicit solver, and 3) post-processing and data analysis to determine stresses on leaflets and stent. Clinically, 29mm SapienXT is recommended for 26–29mm native annulus diameter. Here, two extreme deployed geometries of 26mm and 29mm (nominal diameter) Sapien XT were simulated.

Sapien XT Mesh Generation

Fully expanded, nominal sized SapienXT (29mm) was imaged with desk-top cone-beam micro-computed tomography scanner (microCT-40; Scanco Medical AG, Baseldorf, Switzerland) in different orientations and intensities to distinguish stent and leaflet geometries. Scan settings were 45kVp X-ray energy, 200μA X-ray current, with 0.5mm aluminum filter, 50mm field of view, 50μm voxel at 200ms integration time. High-resolution DICOM (Digital Imaging and Communications in Medicine) images (voxel size 50×50×50μm) were imported into MeVisLab, an open source surface reconstruction software (http://www.mevislab.de/). Stent and leaflet surfaces were combined using suture lines as a reference point for leaflet orientation. Reconstructed surface was then imported into GeoMagic Design, (3D Systems, Rock Hill, SC, USA), an inverse engineering software, to create and refine geometric model with accurate size and thickness at zero stress. Total 27,700 elements were generated in HyperMesh (Altair Engineering, Troy, MI). Commercial explicit FE ABAQUS CAE software (Dassault Systems, Waltham, MA) was used to import FE meshes and apply aortic loading and boundary conditions for TAV.

Mesh sizes chosen for the stent and leaflets were 0.5mm and 0.25mm, respectively after mesh convergence study. Leaflet mesh was refined three times in order to reach stress results that were not affected by mesh size. Number of elements in the leaflet were increased from 4,501 to 7,731 and then to 18,202. Stress results converged when the element number was over 7731 with a variation of 1.2%. Total number of 18,202 elements was used in the leaflet.

Finite Element Analyses

Constitutive Model and Material Properties—TAV stent and leaflets were assigned material properties. SapienXT used leaflets made of specially treated bovine pericardium to resist calcification and that proprietary process was the same as for corresponding surgical Carpentier-Edwards pericardial valves (Edwards Lifesciences, Inc, Irvine, CA). We performed biaxial stretch testing of those surgical valve leaflets to determine material properties of TAV leaflets[19], to avoid destroying SapienXT. Methods of biaxial stretching have been previously described[20]TAV leaflets were assumed to be orthotropic, non-linear hyperelastic materials. Material’s response to stress was described mathematically by a set

of constitutive equations, derived from strain energy function W. Using Fung-type hyperelastic material, W was described as

$$W=\frac{c}{2}[e^{Q}-1]+\frac{1}{D}\left(\frac{J^{2}-1}{2}-\ln J\right)$$

$$Q=\sum_{m=1}^{9}c_{m}E_{ij}E_{kl}$$

where c_m, c, and D, are material parameters, and E_{ij} and E_{kl} are components of Green-Lagrangian strain tensor. Subscripts i, j, k, and l refer to radial, circumferential and longitudinal directions. Material parameters in above equations, obtained from biaxial tensile tests, are listed in Table 1. TAV stent geometry used cobalt-chromium material properties and was modeled using an elastic-plastic material model with Young's modulus 245GPa, Poisson's ratio 0.3, and yield stress 450MPa.

Simulations—FE simulations were performed using ABAQUS solver. Reconstructed TAV is shown in figure 1a. Leaflet thickness was 0.24mm, modeled as mostly 4-sided shell elements. Thickness and width of the wireframe of the stent were 0.65mm and 0.35mm respectively. Stent was meshed into brick solid elements with two elements along the stent thickness(figure 1b). Contact definitions between leaflets and between leaflet and stent were investigated to choose one most accurately representing the overall behavior. Penalty based contact algorithm provided by ABAQUS solver was used to model leaflet contact/coaptation. Leaflets were considered to be in contact with each other when the surface-to-surface distance of the pair of leaflets was less than the leaflet thickness. The coaptation of leaflets was defined as contact pairs with friction coefficient of 0.1. TAV leaflet mesh was sub-divided into 3 distinct regions(figure 1c) to study stress distribution due to pressure loading: 1) upper free edge region, 2) lower belly region and 3) sutured edges. TAV leaflet geometries were sutured to dacron mesh at the bottom and tied to stent geometry at the top(figure 1d). Dacron was sutured to the stent(figure 1e).

Deployed geometry of 26mm diameter was achieved by crimping the fully expanded stent inward to a compressed geometry. Leaflet and dacron, which was sutured to the stent, was also crimped accordingly with the stent. Simulations were performed to determine TAV stresses of different geometries based upon arterial loading conditions on a manufactured TAV without the initial balloon-expansion. Pressure loading was applied to outer surfaces of leaflets and all the surface of the stent to diastolic and systolic pressure with quasi-static loading condition. Initial pressurization featured ramp up from 0mmHg to maximum systolic pressure (120mmHg) or diastolic pressure(80mmHg) over 20ms duration, followed by the constant pressure up to a total 100ms period. Application of pressure in this fashion eliminated any unrealistic inertial forces on TAV and improved numerical stability during simulation. Boundary conditions were thus applied to bottom nodes of the stent to prevent any rigid body motion.

Results

SapienXT 29mm TAV geometry and corresponding FE mesh are shown(figure 1). Loading and boundary conditions were applied to stent and leaflet assembly. Maximum and minimum principal stresses for both nominal 29mm and deployed 26mm SapienXT under diastolic and systolic pressure are shown for quasi-static condition(figures 2–5). For uncompressed nominal 29mm model, maximum principal stresses for TAV stent were 93.31MPa and 129.91MPa at 80 and 120mmHg, respectively(figure 2a,c). Peak stresses occurred at tips of the stents where the motion was confined. Peak stress also occurred at the upper thin stem in the middle between two sutured posts. Minimum principal stresses for TAV stent were −105.60MPa and −147.88MPa at 80 and 120mmHg, respectively(figure 2b,d). These stresses were similarly located at the upper part of the thin long wireframe and where the motion was constrained.

For the leaflets in uncompressed 29mm model, maximum and minimum principal stresses for entire leafletare shown for 80 and 120mmHg under quasi-static condition (figure 3). High stress concentration locations were determined. Maximum principal stresses across entire leaflet were 1.63MPa and 2.39MPa at 80 and 120mmHg, respectively(figure 3a,c). Peak stresses occurred at tips of leaflet commissures along the attachment with the stent as well as the suture line of leaflet to dacron. Minimum principal stresses across entire leaflet were −0.36MPa and −0.47MPa at 80 and 120mmHg, respectively. They also occurred at leaflet commissures(figure 3b,d). Region 3 (sutured edges) contained maximum and minimum principal stresses for entire leaflet(figure 1). Upper free leaflet edges (region 1) had maximum (1.25 and 1.47MPa at 80 and 120mmHg, respectively) and minimum (−0.39 and −0.25MPa at 80 and 120mmHg, respectively) principal stresses in the region where leaflets came into contact around commisure at end diastole. Lower leaflet belly (region 2) had lower maximum (0.93and 1.23MPa at 80 and 120mmHg, respectively) and minimum (−0.05 and −0.08MPa at 80 and 120mmHg, respectively) principal stresses, and stress distribution was evenly distributed. TAV simulations with and without stent are presented as supplemental files online (videos 1–2).

For deployed compressed 26mm model, maximum principal stresses for stent were 526.1MPa and 526.5MPa at 80 and 120mmHg, respectively(figure 4a,c). Peak stresses occurred where leaflet was sutured to the stent. Peak stress also occurred in the middle of the thin stem and posts along the height of the TAV. Minimum principal stresses for TAV stent were −902.1MPa and −902.2MPa at 80 and 120mmHg, located at the opposite surfaces of the maximum principal stress locations(figure 4b,d). Magnitude of peak stress did not change greatly from diastole to systole but was significantly higher than that in uncompressed stent.

For leaflets in the compressed 26mm model, maximum principal stresses were 1.55MPa and 1.74MPa at 80 and 120mmHg, respectively(figure 5a,c). Peak stresses occurred at tips of leaflet commissures along the attachment with the stent as well as the suture line of leaflet to dacron. Minimum principal stresses across entire leaflet were −0.63MPa and −1.04MPa at 80 and 120mmHg, respectively. They also occurred at the same locations of the maximum principal stress(figure 5b,d). Maximum principal stresses were lower than that of

uncompressed leaflets while minimum principal stress (compression/bending stress), was higher than that of uncompressed leaflets. Leaflets had maximum in-plane deformation(strain) in the middle of the commissure and minimum deformation in the belly area(figure 6).

Comment

We demonstrated that maximum and minimum principal stresses in 29mm Sapien XT occurred at stent tips where stent motion was constrained. For leaflets, maximum and minimum principal stresses occurred at commissures where leaflets attached to the stent. These regions would be areas most prone to initiating degeneration. Clinically, balloon-expandable TAVR has shown equipoise with SAVR at 5 years in randomized trials(1), while self-expanding TAVR had lower mortality than SAVR in the short-term[5]. Now that PARTNER II has demonstrated TAVR equipoise with SAVR in intermediate-risk patients[6], issues of TAVR durability will become paramount in younger and lower-risk patients.

Durability is the Achilles heel of tissue heart valves, whether TAVR or SAVR. Tissue valve durability is influenced primarily by structural valve dysfunction, resulting from bioprosthetic valve degeneration. Pathologically, bioprosthetic degeneration involves leaflet cusp calcification and stiffening, and leaflet tearing[21]. The rate of bioprosthetic degeneration is influenced by: 1) patient factors, 2) valve leaflet biomaterials, and 3) valve design[21]. While the mechanism of degeneration is poorly understood and multifactorial, patient age is known to significantly impact degeneration with shorter valve durability, the younger the patient age at time of valve implantation. Patient age, hemodynamics (i.e. patient-prosthesis mismatch), and immunologic response may potentially interact to play a role in bioprosthetic durability[22]. Thus, the TAVR durability demonstrated in octagenarians in clinical trials will not be expected to directly translate into durability if TAVR moves into younger healthier surgical patients.

Second factor influencing durability relates to valve leaflet biomaterials. Leaflet composition, gluteraldehyde fixation, and anticalcification treatments are all vitally important for structural integrity as well as determining leaflet mineralization response[21]. Biomaterials for surgical bioprostheses mainly consist of bovine pericardium, porcine valve leaflets, and human allograft leaflets. TAVs are also comprised of similar leaflet materials, bovine, equine, porcine pericardium or porcine valve leaflets[8]. Both bovine pericardium and porcine leaflets have a long history of use and predictable durability in surgical bioprostheses. However, as TAVR delivery systems reduced catheter size to 14–18Fr, much thinner pericardium must be utilized in TAVs than bioprostheses[9,10]. Thinner leaflets would be expected to increase leaflet stress and impact durability. For Sapien XT, bovine pericardium and treatment processes were similar to Edwards surgical bioprostheses with the exception of leaflet thickness. As such Sapien XT leaflet material properties were taken from those of Edwards surgical bioprostheses; however, exact leaflet thickness from SapienXT geometry was used.

Third factor influencing valve durability is valve design which arguably may be the greatest difference among TAVRs and between TAVR and SAVR[9]. For surgical bioprostheses,

degeneration by calcification or leaflet tearing correlated with areas of high tensile and compressive stresses[23,24], and cyclic flexural fatigue and bending[25,26]. Previously, 25mm Edwards bovine pericardial valve was investigated by FEA, using those valves' leaflet material properties and exact valve geometry under 120mmHg quasi-static loading conditions[24]. Maximum in-plane stress ranged from 544.7 to 663.2kPa, though leaflet and stent interaction were not specified. Leaflet stresses were greatest near the commissures and least near the free edge. Our maximum principal stress was higher for 29mm SapienXT than that reported for bioprosthesis. Dynamic FEA simulation of 23mm bovine pericardial Edwards bioprosthesis using physiologic arterial pressures demonstrated peak von Mises stress of 2.09MPa located at the cuspal commissures in the fully closed position[26]. Since bioprosthetic valve sizes in these studies were smaller than our TAV size, direct comparisons are not possible since larger valve sizes may have higher leaflet stresses. Nonetheless, our data suggests higher leaflet stresses in TAVs than bioprostheses, which occurred in similar locations, cuspal commissures.

Comparison with TAV Simulations

Comparison to previous simulation work on stress analysis of TAV valves is presented in Table 2. We report greater leaflet stresses than their studies, which may reflect our larger TAV diameter, exact leaflet geometry and thickness, as well as incorporation of TAV stent and Dacron with leaflet interactions in our simulations. Thinner leaflets resulted in higher stresses and peak stresses occurred along leaflet-stent attachment along the commissures[10]. Other groups have reported fatigue simulations using surgical leaflets of 25mm Carpentier-Edwards pericardial valve and 23mm generic TAV leaflets[27]. Stress was significantly higher in smaller TAV leaflets than larger surgical valve leaflets. They predicted TAV durability to 7.8 years. However, neither of these studies utilized exact geometry and fully assembled TAVR including leaflets, stent, Dacron, and sutures. In our study, when examining 29mm SapienXT at nominal vs compressed to 26mm within patient's annulus, underexpansion of TAVR resulted in significantly higher stent stresses. With regards to the leaflets, peak first principal stresses were higher in the compressed state while peak second principal stresses were lower. The counter effects of higher tensile stresses but lower compressive or bending stresses on leaflet durability are presently unknown.

Study Limitations

Our study did not take into account crimping and ballooning process which occurs during TAVR. Crimping physically damages TAV leaflets and may weaken leaflets and increase leaflet stress[28,29]. We did not destroy our TAV to test its leaflets for exact material properties given the rarity of obtaining TAVs and need for future TAV experimental *in vitro* testing. As such we utilized excised leaflets from Edwards' surgical bioprostheses to determine material properties for TAV leaflets. While treatment processes for both Edwards valves are expected to be the same, thinner pericardial leaflets used in TAVR may have different material properties than were represented here. This study was performed with quasistatic simulation to determine maximal leaflet and stent stresses. A dynamic simulation to examine in detail, leaflet coaptation was not performed. As stress at sites of leaflet coaptation were significantly less than the commissures which demonstrated peak stress, dynamic simulation would not likely change the results of the present study. Future work on

leaflet coaptation may be performed. Since stent and leaflet stresses cannot be directly measured, our analyses of stress cannot be experimentally validated. Determinations of strain experimentally are beyond the scope of this work and will be considered for future studies. Lastly, complex fluid-structure interaction simulations were not incorporated and beyond the present scope of this study.

Conclusions

We determined TAV stent and leaflet stresses on SapienXT 29mm using exact geometry. We demonstrated that maximum stresses occurred at tips of the stent where motion was constrained and at leaflet commissures where they attached to the stent. These leaflet regions will likely be areas where degeneration initiates.

Supplementary Material

Refer to Web version on PubMed Central for supplementary material.

Acknowledgments

The study was funded by University of California Proof of Concept grant #246590 and National Institutes of Health, R01HL119857-01A1.

References

1. Nishimura RA, Otto CM, Bonow RO, et al. 2014 AHA/ACC Guideline for the Management of Patients With Valvular Heart Disease: a report of the American College of Cardiology/American Heart Association Task Force on Practice Guidelines. Circulation. 2014; 129(23):e521–643. [PubMed: 24589853]
2. Kapadia SR, Leon MB, Makkar RR, et al. 5-year outcomes of transcatheter aortic valve replacement compared with standard treatment for patients with inoperable aortic stenosis (PARTNER 1): a randomised controlled trial. Lancet. 2015
3. Mack MJ, Leon MB, Smith CR, et al. 5-year outcomes of transcatheter aortic valve replacement or surgical aortic valve replacement for high surgical risk patients with aortic stenosis (PARTNER 1): a randomised controlled trial. Lancet. 2015
4. Popma JJ, Adams DH, Reardon MJ, et al. Transcatheter aortic valve replacement using a self-expanding bioprosthesis in patients with severe aortic stenosis at extreme risk for surgery. Journal of the American College of Cardiology. 2014; 63(19):1972–1981. [PubMed: 24657695]
5. Adams DH, Popma JJ, Reardon MJ, et al. Transcatheter aortic-valve replacement with a self-expanding prosthesis. The New England journal of medicine. 2014; 370(19):1790–1798. [PubMed: 24678937]
6. Leon MB, Smith CR, Mack MJ, et al. Transcatheter or Surgical Aortic-Valve Replacement in Intermediate-Risk Patients. The New England journal of medicine. 2016
7. Thyregod HG, Steinbruchel DA, Ihlemann N, et al. Transcatheter Versus Surgical Aortic Valve Replacement in Patients With Severe Aortic Valve Stenosis: 1-Year Results From the All-Comers NOTION Randomized Clinical Trial. Journal of the American College of Cardiology. 2015; 65(20): 2184–2194. [PubMed: 25787196]
8. Tchetche D, Van Mieghem NM. New-generation TAVI devices: description and specifications. EuroIntervention: journal of EuroPCR in collaboration with the Working Group on Interventional Cardiology of the European Society of Cardiology. 2014; 10(Suppl U):U90–U100.
9. Tseng EE, Wisneski AD, Azadani AN, Ge L. Engineering perspective on transcatheter aortic valve implantation. Interv Cardiol. 2013; 5(1):53–70.

10. Li K, Sun W. Simulated thin pericardial bioprosthetic valve leaflet deformation under static pressure-only loading conditions: implications for percutaneous valves. Annals of biomedical engineering. 2010; 38(8):2690–2701. [PubMed: 20336372]
11. Sun W, Li K, Sirois E. Simulated elliptical bioprosthetic valve deformation: implications for asymmetric transcatheter valve deployment. Journal of biomechanics. 2010; 43(16):3085–3090. [PubMed: 20817163]
12. Abbasi M, Azadani AN. Leaflet stress and strain distributions following incomplete transcatheter aortic valve expansion. Journal of biomechanics. 2015; 48(13):3663–3671. [PubMed: 26338100]
13. Wang Q, Sirois E, Sun W. Patient-specific modeling of biomechanical interaction in transcatheter aortic valve deployment. Journal of biomechanics. 2012; 45(11):1965–1971. [PubMed: 22698832]
14. Wang Q, Kodali S, Primiano C, Sun W. Simulations of transcatheter aortic valve implantation: implications for aortic root rupture. Biomechanics and modeling in mechanobiology. 2015; 14(1): 29–38. [PubMed: 24736808]
15. Capelli C, Bosi GM, Cerri E, et al. Patient-specific simulations of transcatheter aortic valve stent implantation. Med Biol Eng Comput. 2012; 50(2):183–192. [PubMed: 22286953]
16. Morganti S, Conti M, Aiello M, et al. Simulation of transcatheter aortic valve implantation through patient-specific finite element analysis: two clinical cases. Journal of biomechanics. 2014; 47(11): 2547–2555. [PubMed: 24998989]
17. Russ C, Hopf R, Hirsch S, et al. Simulation of transcatheter aortic valve implantation under consideration of leaflet calcification. Conference proceedings : Annual International Conference of the IEEE Engineering in Medicine and Biology Society IEEE Engineering in Medicine and Biology Society Annual Conference. 2013; 2013:711–714.
18. Bailey J, Curzen N, Bressloff NW. Assessing the impact of including leaflets in the simulation of TAVI deployment into a patient-specific aortic root. Computer methods in biomechanics and biomedical engineering. 2015:1–12.
19. Kuang H, Xuan Y, Lu M, et al. Leaflet Mechanical Properties of Carpentier-Edwards Perimount Magna Pericardial Aortic Bioprostheses. Journal of Heart Valve Disease. In press.
20. Azadani AN, Chitsaz S, Matthews PB, et al. Comparison of mechanical properties of human ascending aorta and aortic sinuses. Ann Thorac Surg. 2012; 93(1):87–94. [PubMed: 22075218]
21. Schoen FJ, Levy RJ. Calcification of tissue heart valve substitutes: progress toward understanding and prevention. The Annals of thoracic surgery. 2005; 79(3):1072–1080. [PubMed: 15734452]
22. Johnston DR, Soltesz EG, Vakil N, et al. Long-term durability of bioprosthetic aortic valves: implications from 12,569 implants. The Annals of thoracic surgery. 2015; 99(4):1239–1247. [PubMed: 25662439]
23. Vesely I. The evolution of bioprosthetic heart valve design and its impact on durability. Cardiovasc Pathol. 2003; 12(5):277–286. [PubMed: 14507578]
24. Sun W, Abad A, Sacks MS. Simulated bioprosthetic heart valve deformation under quasi-static loading. J Biomech Eng. 2005; 127(6):905–914. [PubMed: 16438226]
25. Martin C, Sun W. Simulation of long-term fatigue damage in bioprosthetic heart valves: effects of leaflet and stent elastic properties. Biomechanics and modeling in mechanobiology. 2014; 13(4): 759–770. [PubMed: 24092257]
26. Kim H, Lu J, Sacks MS, Chandran KB. Dynamic simulation of bioprosthetic heart valves using a stress resultant shell model. Annals of biomedical engineering. 2008; 36(2):262–275. [PubMed: 18046648]
27. Martin C, Sun W. Comparison of transcatheter aortic valve and surgical bioprosthetic valve durability: A fatigue simulation study. Journal of biomechanics. 2015; 48(12):3026–3034. [PubMed: 26294354]
28. Kiefer P, Gruenwald F, Kempfert J, et al. Crimping may affect the durability of transcatheter valves: an experimental analysis. The Annals of thoracic surgery. 2011; 92(1):155–160. [PubMed: 21718842]
29. Alavi SH, Groves EM, Kheradvar A. The effects of transcatheter valve crimping on pericardial leaflets. The Annals of thoracic surgery. 2014; 97(4):1260–1266. [PubMed: 24444873]

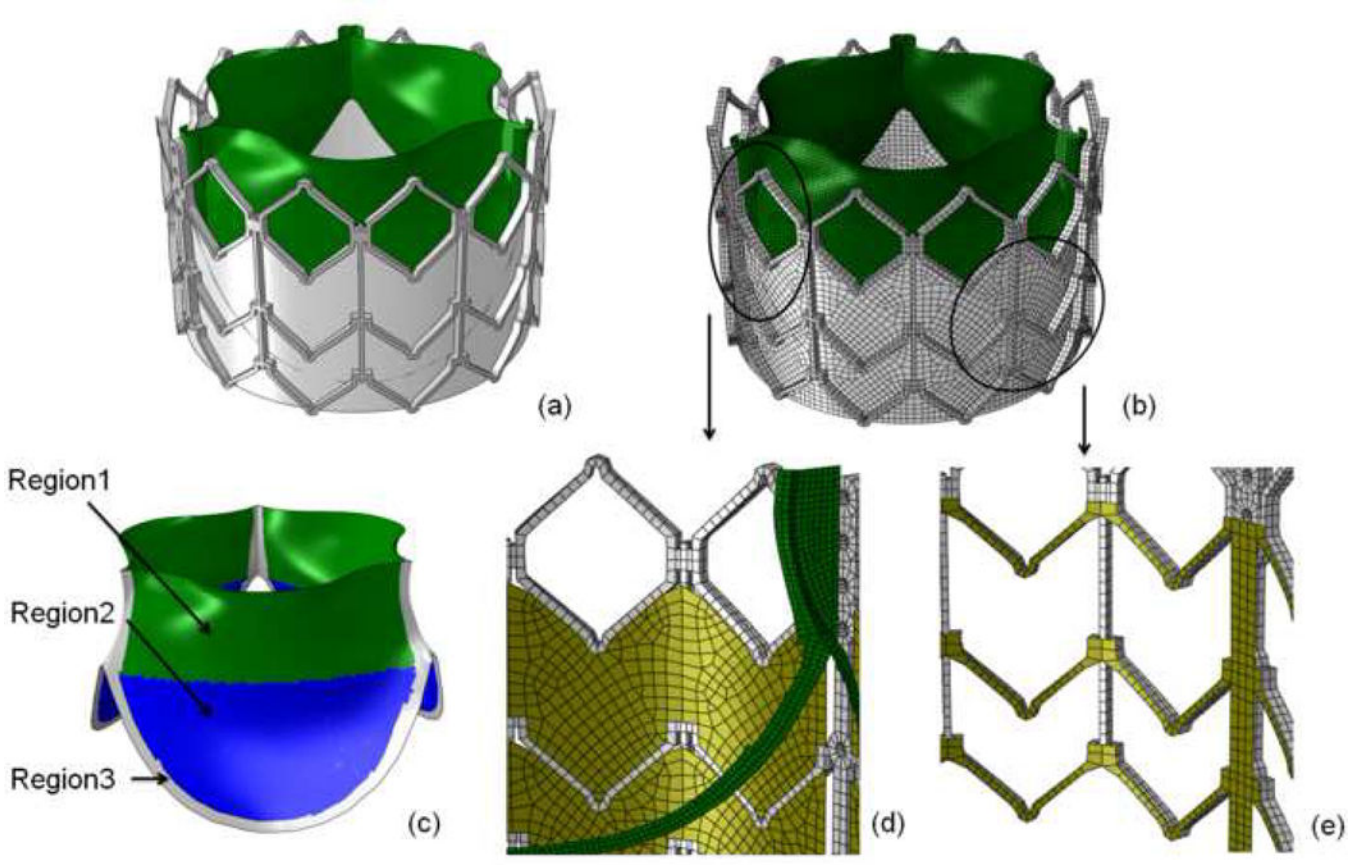

Figure 1.

a) Geometry of 29mm SapienXT. b) Finite element meshes of 29mm SapienXT. c) Regions of interest:region 1=upper leaflet free edges; region 2=lower leaflet belly; and region 3=sutured leaflet edges. d) Mesh of leaflet sutured to stent and dacron. e) Mesh of dacron sutured to stent.

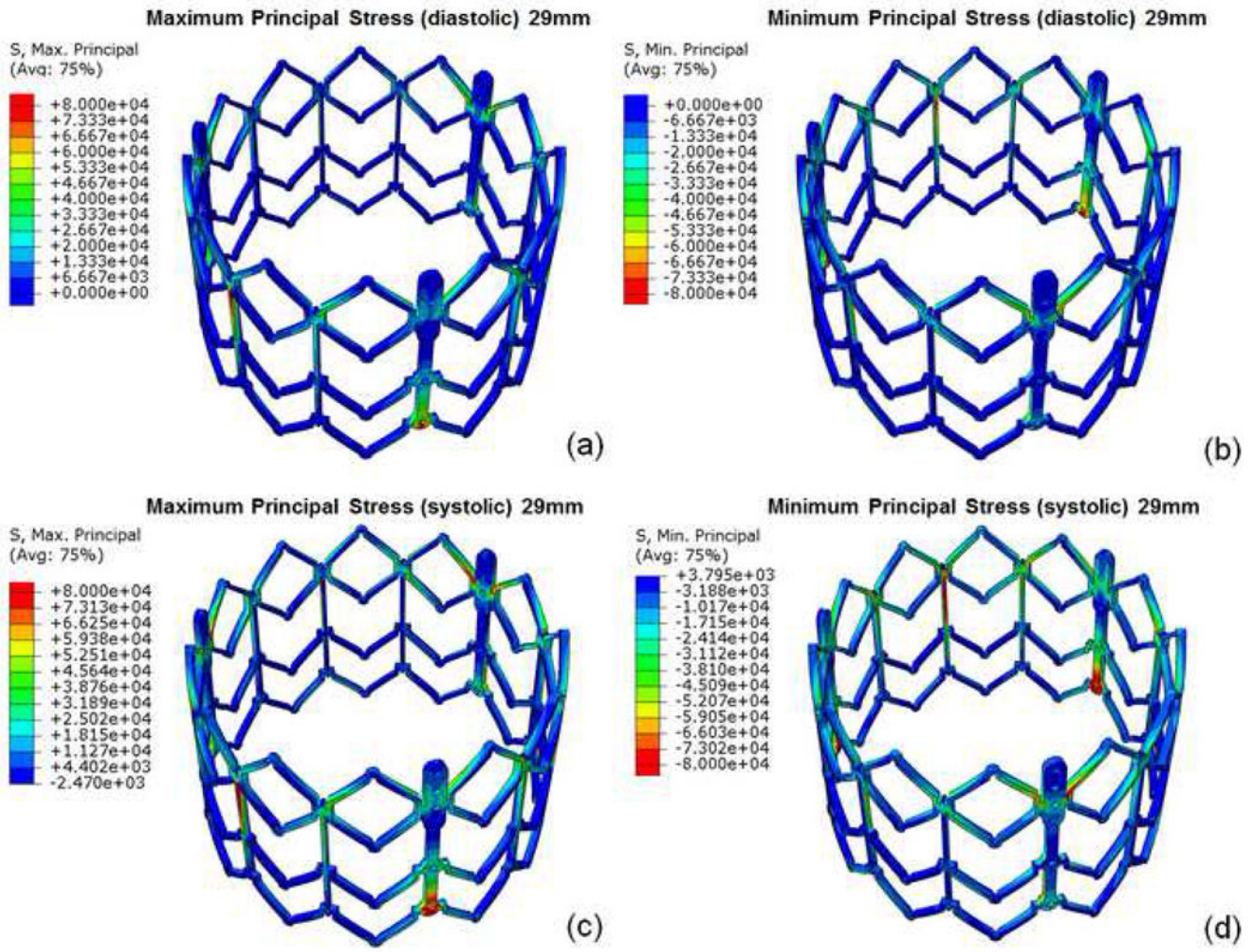

Figure 2.

For 29mm SapienXT, a) maximum and b) minimum principal stresses of stent at diastole and c) maximum and d) minimum principal stresses at systole.

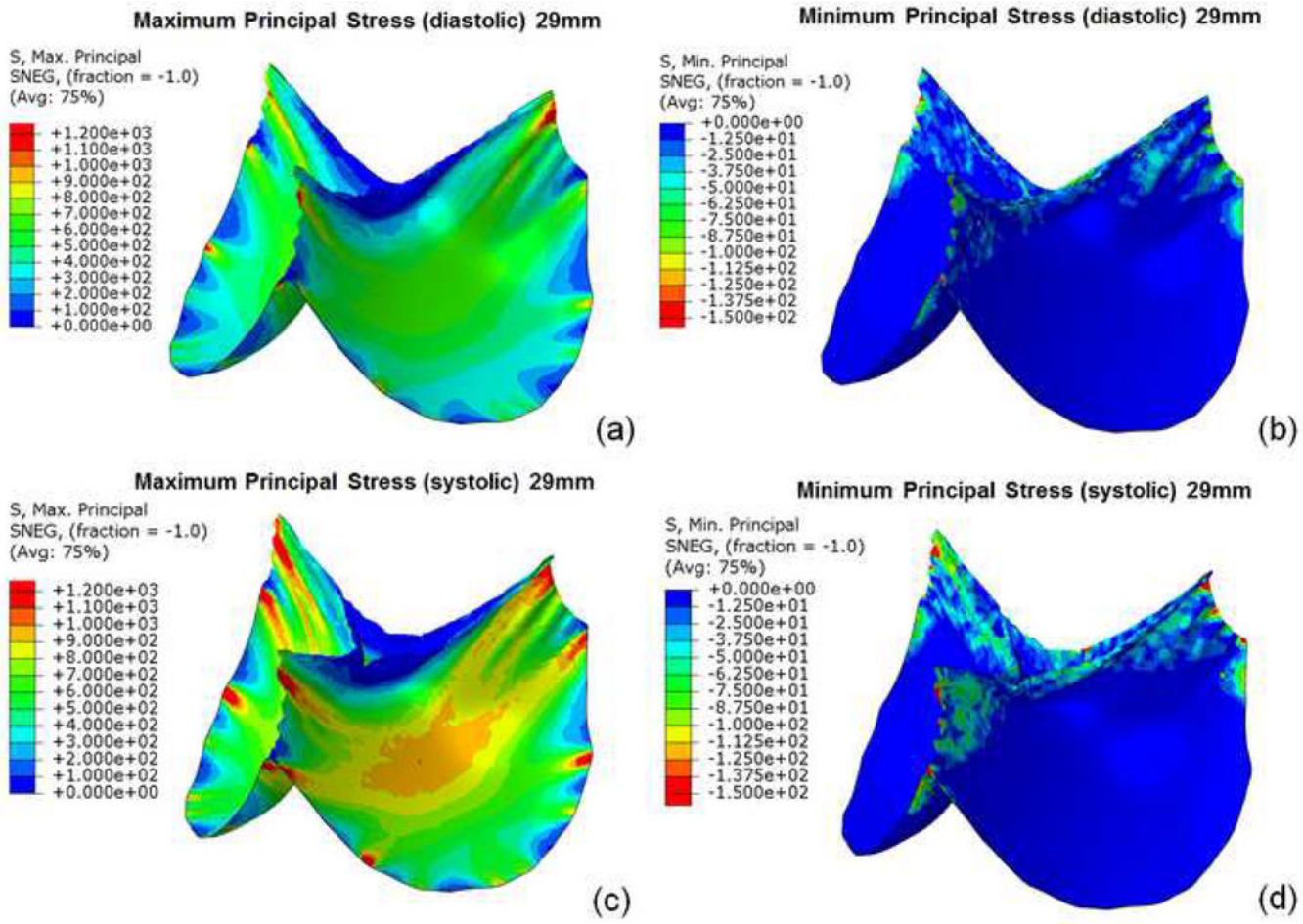

Figure 3.

For 29mm SapienXT, a) maximum and b) minimum principal stresses on leaflets at diastole and c) maximum and d) minimum principal stresses at systole.

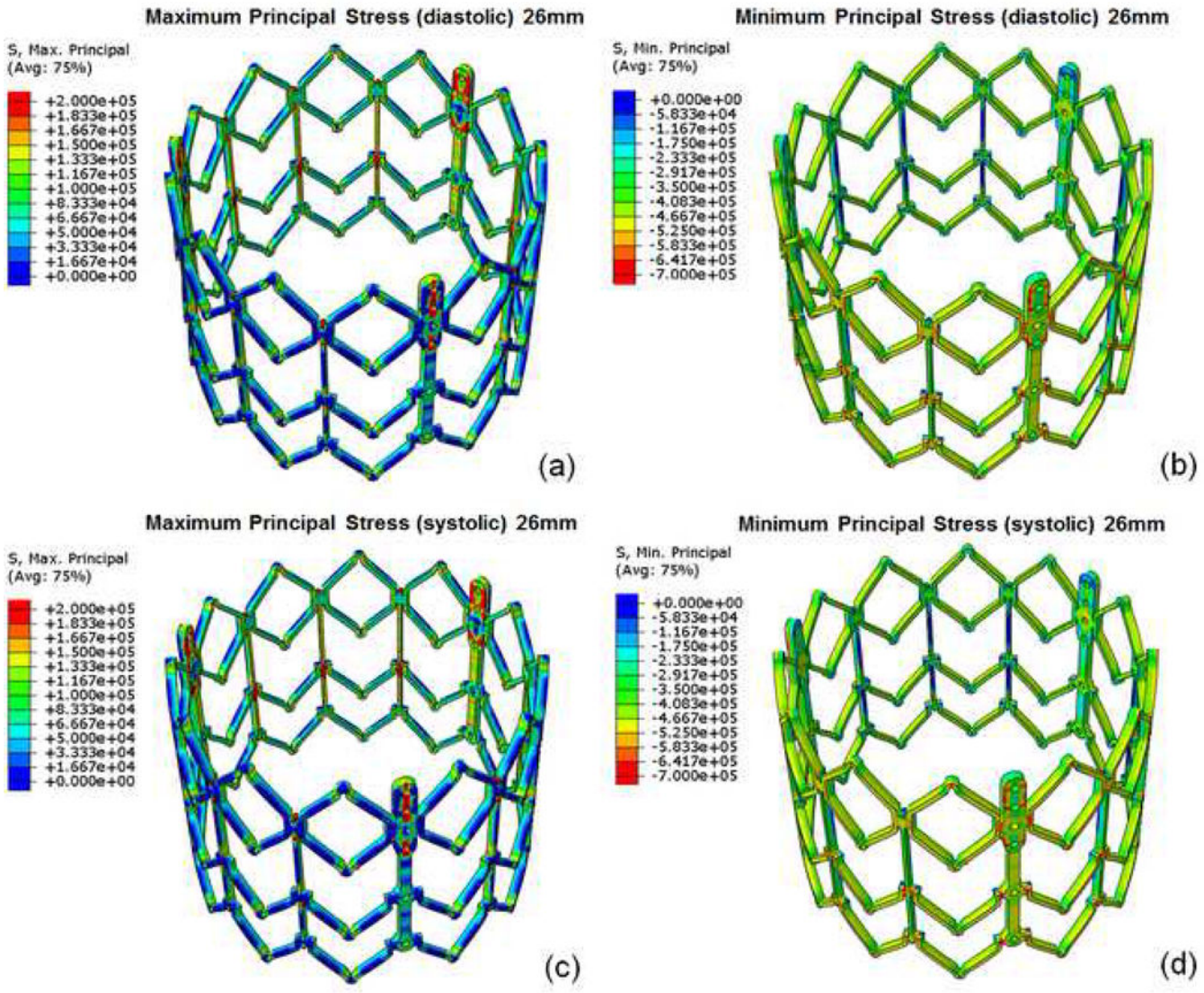

Figure 4.

For compressed 26mm SapienXT, a) maximum and b) minimum principal stresses of stent at diastole and c) maximum and d) minimum principal stresses at systole.

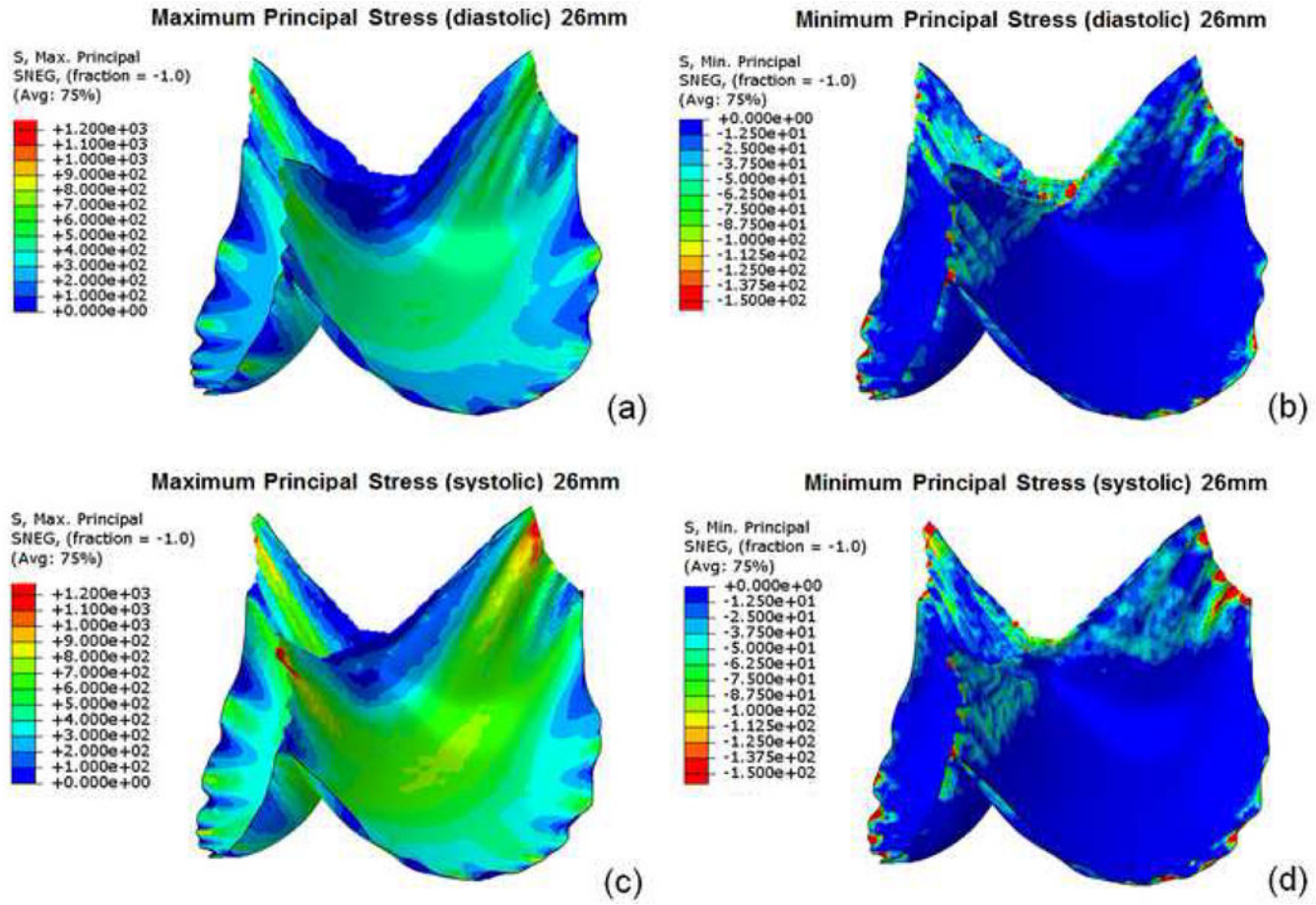

Figure 5.

For compressed 26mm SapienXT, a) maximum and b) minimum principal stresses on leaflets at diastole and c) maximum and d) minimum principal stresses at systole.

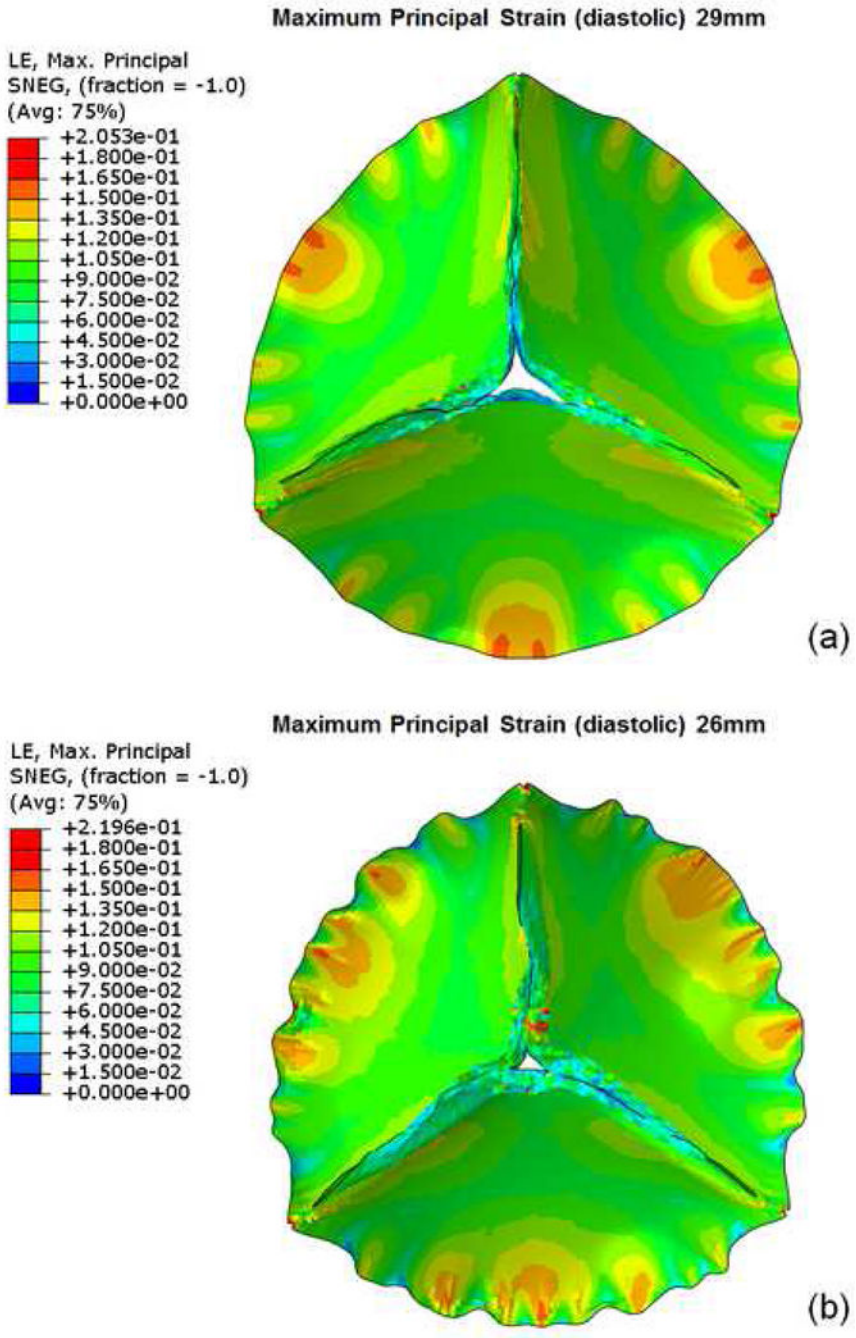

Figure 6.
Maximum principal strain of a) 29mm and b) 26mm Sapien XT under diastolic pressure.

Table 1

Material constants for leaflets and stent.

c_1	c_2	c_3	c_4	c_5	c_6
62.28	26.97	132.12	0.01	0.01	0.01
c_7	c_8	c_9	c	D	
31.14	0.01	0.01	5.01	0.000001	

Table 2

Previous simulation of TAVs.

Geometry	Diameter	Bioprothesis	Peak Principal Stress	Pressure/Load	Reference
Estimated	22mm	Bovine	0.92MPa	120mmHg	[10]
Estimated	22mm	Porcine	1.57MPa	120mmHg	[10]
Homemade	23mm	Bovine	2.52MPa	100mmHg	[12]
Perimount	25mm	Bovine	1.5MPa	23N	[27]
Estimated	23mm	Bovine	1.5MPa	9N	27]